Full waveform LiDAR for adverse weather conditions

Full Waveform LiDAR for Adverse Weather Conditions

Andrew M. Wallace, Abderrahim Halimi, and Gerald S. Buller

***Abstract*—We present and discuss the case for full waveform pixel and image acquisition and processing to enable LiDAR sensors to penetrate and reconstruct 3D surface maps through obscuring media. To that end, we review work on signal propagation, on scanning and arrayed sensors, on signal processing strategies for independent pixels and employing spatial context, on reducing complexity and accelerating processing by sensor design, algorithmic changes, compressed sensing, and parallel processing. We report several experimental studies on LiDAR imaging through complex media, and how these can inform the automotive LiDAR scenario. We conclude with a discussion of future development and potential for full waveform LiDAR (FWL).**

***Index Terms*—Automotive LiDAR, full waveform LiDAR, obscuring media, bad weather, signal propagation, scene reconstruction, discussion paper.**

I. Introduction

CURRENT automotive sensing systems designed for either full autonomy or driver assistance employ a multimodal suite of disparate sensors for scene mapping and classification of other road users, of which passive optical cameras, LiDAR and radar are usually the main components [1]. As these sensors have complementary strengths and weaknesses, sensor fusion [2]–[4] is often applied to acquire high resolution images at near to far ranges in both favourable and unfavourable viewing conditions. However, fusion of disparate sensing systems with different fields of view, acquisition rates, resolutions, and error models is not trivial.

In this discussion paper, we make the case for full waveform LiDAR (FWL) in its own right and as a key component of sensor fused systems. We argue that new developments in solid state LiDAR and in FWL data processing mean that we can now consider LiDAR signals to have a penetrative capability through obscuring media, and so move closer towards radar performance in bad weather while retaining the advantages of high spatial resolution. Further, as both radar and FWL provide continuous data on reflected power as a function of range, this opens up new research in full waveform fusion that goes beyond the current state of the art. We provide illustrations from our own and other researchers' work on FWL, and follow this with a summary and discussion of the necessary steps to make FWL automotive sensing a reality.

Fig. 1. The sensor suite and the test vehicle. This includes from left to right (Inset), a Velodyne HDl-32E LiDAR a Zed Stereo Camera pair and a Navtech-CIR104 79 GHz radar system.

II. LiDAR, Radar and Passive Optical Automotive Sensing

Although a modern car has many types of sensor [1], we concentrate on those capable of the two key functions for situational awareness, scene mapping and object recognition using a-priori information provided by GPS and/or IMU systems if available. Currently we employ a test vehicle to map the environment in all weathers, fusing data from radar, LiDAR and optical stereo sensors as shown in Fig. 1. However, the LiDAR sensor is a limited, single or dual pulse system, typical of the automotive context [5], [6]. We do not have FWL data available on this vehicle; an example of concurrent multimodal data acquisition is shown in Fig. 2. The main concentration for LiDAR technology has been on scene mapping; deep neural networks have been lauded for their success in recognizing objects in video data (see [7] for competitive results on automotive benchmarks), but this does not yet translate to results on objects appearing in LiDAR (or indeed radar) data.

Manuscript received October 21, 2019; accepted April 1, 2020. Date of publication April 22, 2020; date of current version July 16, 2020. This work was supported in part by the Engineering and Physical Research Council, under Grants EP/N012402/1 (TASCC: Pervasive low-TeraHz and Video Sensing for Car Autonomy and Driver Assistance (PATH CAD), EP/S000631/1 (Signal Processing for the Information Age) and EP/N003446/1 (Next Generation Imaging using Sparse Single-Photon Data), and in part by The U.K. Defence Science and Technology Laboratory under Grants EP/S000631/1 and DSTL X1000114765. The work of Abderrahim Halimi was supported by the Royal Academy of Engineering Fellowship under Grant RF/201718/17128. The review of this article was coordinated by Prof. F. Lavagetto. *(Corresponding author: Andrew Wallace.)*

The authors are with the School of Engineering and Physical Sciences, Heriot-Watt University, Edinburgh EH14 4AS, U.K. (e-mail: a.m.wallace@hw.ac.uk; a.halimi@hw.ac.uk; g.s.buller@hw.ac.uk).

Digital Object Identifier 10.1109/TVT.2020.2989148

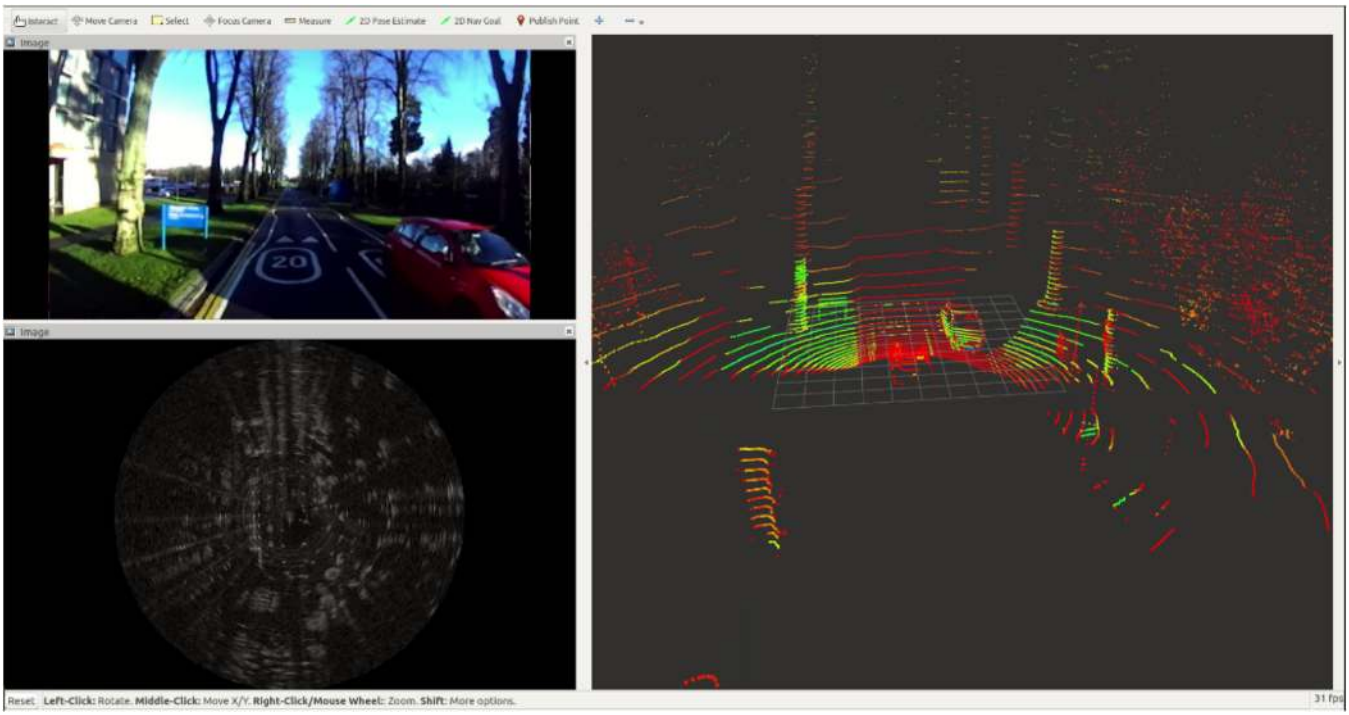

Fig. 2. Examples of instantaneous video, radar and LiDAR images acquired by the field trials vehicle of Fig. 1. The images were taken around Edinburgh in clear weather and the radar and optical stereo image scan be used identify targets (e.g. other vehicles) and correspondences can be made between the different modalities. The LiDAR image is restricted in range, and demonstrates that we need more sensitive processing of full waveform data.

Even in good conditions, there are a number of limiting factors to the deployment of LiDAR systems for autonomy and driver assistance. In principle the resolution can be sub-cm in range and cross-range as the collimated beam diameter divergence is small, but such fine cross range resolution implies very dense pixel arrays or fine scanning, and results in very large datasets. A typical current, commercial LiDAR system may produce in excess of 1,000,000 depth points per second, assuming a single or a dual return per transmitted pulse. If we move to FWL, this increases dramatically, depending on the distance resolution. So, there are data bandwidth and storage [8] issues. The vehicle must be able to see sufficiently far ahead to take appropriate action, but LiDAR systems must be eye safe, setting limits on laser power, and hence maximum range. A proposed specification from one manufacturer is for a 905 nm wavelength solid-state LiDAR with a range of 150 m at 8% surface reflectivity [5], although we have not been able to achieve this with our existing sensors. Future systems also need to be immune from interference (from other vehicles) and malicious attack [9], necessitating more complex signal filtering and coding strategies.

What of other sensing modalities? Passive optical sensors can acquire 3D images from disparity analysis, but as there is no direct light source this depends on detail in the scene, the depth resolution is poor and varies with range. The intensity response is integrated over the optical path, so there is no current possibility of discriminative (by depth) optical processing for 'seeing through fog'. Automotive radar systems [10] perform much better in adverse weather, and have much longer range, typically up to ≈300 m. Although they can have good resolution in depth due to the high bandwidths in the 24 GHz–300 GHz range [11], the image plane resolution is poor due to the wide beam divergence. Especially in elevation, the data is effectively discarded and a range bearing map is produced rather than a full 3D image. Recent research in low THz imaging in particular aims to address these limitations, and super resolution and interferometric depth techniques [12] may give genuine 3D radar data at much better resolution in all dimensions. However, it will be some time before this approaches LiDAR resolution.

Hence, we evaluate the issues concomitant with a move from single return to FWL for operation in adverse weather conditions, such as fog, rain, snow and mist. To that end, we consider signal propagation, processing strategies, what lessons can be learnt from experimental studies of FWL imaging through obscuring media, and issues of sensor design and software and hardware algorithmic complexity. This does not contradict the probable need for fusion of radar and optical data, but simply asks the question whether 'clever' processing of FWL data can make a valuable contribution to acquire more detailed 3D scene maps in adverse conditions.

III. Laser Signal Transmission in Bad Weather

A. Attenuation and Scattering of the Signal

Adverse conditions for automotive LiDAR can include rain, snow, hail, mist, fog, smoke, and spray from the road surface. Working from the basic laser radar equations [13], [14], the designer has to factor in a wide dynamic range of return signal strengths based on not just reflectivity but also on attenuation. Traditionally, the four main wavelengths for study of land based, sub-10 km sensing LiDAR have been near the

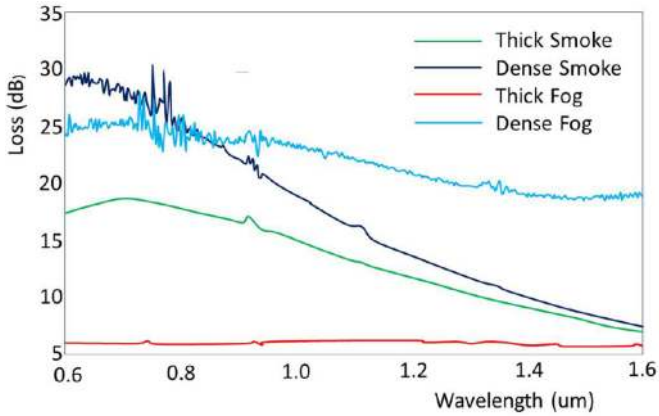

Fig. 3. A comparison of attenuation loss in Fog and Smoke in the visible and near infrared [19]. Here dense smoke is defined as having visibility < 0.07 km, thick smoke < 0.5 km. These experiments were carried out in a controlled atmospheric chamber of length 550 cm. (©2012 IEEE).

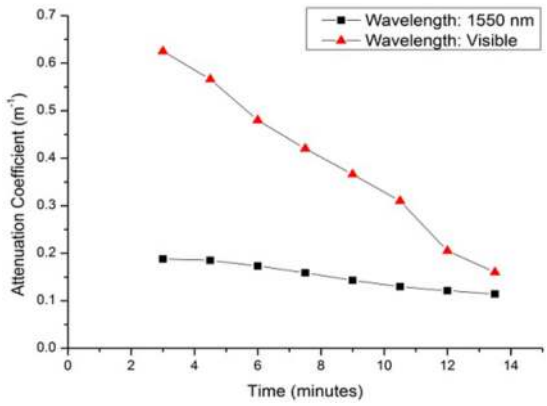

Fig. 4. Comparison of attenuation coefficient of glycol-based smoke at visible and 1550 nm wavelengths as smoke disperses [29]. The key observation is the significantly reduced attenuation at 1550 nm.

1 μm, 1.5 μm, 2 μm and 10.6 μm wavelengths [15], of which the sub-1 μm waveband has the advantage of falling within the detection range of widely available silicon-based optical technology [16]. Light can propagate through the human eye to the retina, which is unsafe, especially at visible wavelengths, so that 1.5 μm is more suitable, although this necessitates the more expensive and less integrated Indium Gallium Arsenide (InGaAs) based detectors.

Theoretical scattering models (Rayleigh, Mie, Geometric) depend on the relative size of the wavelength and the atmospheric particles [17], and as there is no benchmark for what is adverse, there is disagreement between different experimental studies, and between theory and experiment. Experimental investigations usually focus on fog and smoke in controllable conditions using machines or canisters [18]–[22]. Light propagation at 1550 nm may suffer less from attenuation by obscurants than at shorter wavelengths, but Kim *et al.* [17] suggested that this conclusion was true in haze, but not necessarily in fog, based on theoretical modeling and a meta-analysis of the literature. Fig. 3 shows examples of the attenuation loss in different densities of fog and smoke, showing an advantage for the higher wavelength in dense smoke, but not fog. Similar studies and comparisons between experiment and theory in fog and rain were conducted by Rasshofer *et al.* [14] and Khan *et al.* [20].

Explicit studies on automotive LiDAR at the two wavelengths of 905 nm and 1550 nm have been conducted [23], [24] and compared to a 24 GHz radar in [23]. The main metric was target detection. The conclusions confirm the other studies; they considered it advantageous to use 1550 nm, not because of differences in attenuation, but because the higher wavelength allows significantly higher power while maintaining eye safety. As regards the radar, they noted that resolution and classification were poor, and very dependent on the target material.

Most of these studies tended to focus on relatively reproducible pollutants rather than snow or rain which are harder to characterize. Fersch *et al.* [25] did consider the influence of discrete rain drops on a pulsed LiDAR but this really only looked at rain on the aperture and they concluded the effect was non-critical in reducing power. Trierweiler *et al.* [26] discussed steps to both detect and remove the presence of contaminants on sensors and any signal effect of very near-field distortion in the signal can be effectively gated in many cases.

Our own trials [27] included verification of point-to-point propagation measurements using a TCSPC LiDAR at a wavelength of 1550 nm through several obscuring media, water fog, smoke generated from a glycol smoke machine and white smoke from canisters. Calibration targets were used to give an independent visibility estimate [20] so that the attenuation length of the medium could be calculated. The tunnel was filled initially then the obscuring medium slowly dispersed, and images were acquired at 2 minute intervals, as shown in Fig. 4 for glycol-based smoke. These results confirm that the 1550 nm wavelength is potentially advantageous for certain obscuring media, as in Fig. 4, but not all, and improves eye safety. Satat *et al.* [28] did similar experiments to recover single target surfaces through fog, to which we shall return in Section V.

The study of Pfennigbauer *et al.* [22] is instructive. The experimental environment was similar to [29], but they recorded a FWL measurement through all the obscuring medium between the sensor and the target, not gating the results around an a-priori target position [29]. For an automotive LiDAR, this is necessary because objects of interest are distributed in depth, a near pedestrian, a distant car and so on. There are two key observations. At 40 m visibility (Fig. 5), the majority of the returned signal is from the intervening medium, and further there are significant peaks due, presumably, to inhomogeneous volumes in a relatively sparse medium. At 10 m visibility (not shown), the intervening medium is homogeneous, but the target is barely visible, if at all. Hence we argue later in this paper for more advanced processing strategies that take into account a significant presence of outliers, spatial constraints between adjacent pixels, and modeling of the medium itself.

Recently, an extensive study by Carballo *et al.* [30] examined the performance of 12 different LiDAR sensors to capture the range accuracy and density of scenes in a 200 meter weather chamber, simulating rainy and foggy conditions. This, too, is instructive, showing false returns generated by intervening fog

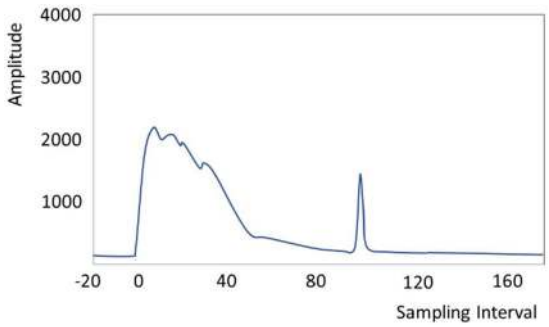

Fig. 5. Example of imaging a black and white planar target in fog with visibility of 40 m from [22]. The path length was 30 m. Similar data can be found in [23] and [28].

and rain that confuse the LiDAR sensors to detect false targets, and additional interference effects when using multiple LiDARS simultaneously. Zhao *et al.* [31] developed an automotive simulation package that includes geometric modelling, attenuation using the laser radar equation, and a probabilistic model for reflection from homogeneously distributed raindrops. Outdoor validation tests were performed, but because these were uncontrolled these provided only intuitive comparisons with the simulated data. Although very instructive, these latter studies use commercial systems that operate on the single echo principle, and as such reinforce the necessity for full waveform processing presented here.

Attenuation is not the only concern; turbulence can produce wind affected, time varying refractive gradients that can create scintillation, beam spreading and wander [15], which is particularly noticeable on short time exposures. The majority of the studies have been directed at long distance optical communication, e.g. [32]. The effect of such adversarial conditions has not been systematically studied in an automotive context where established benchmarks tend to provide good weather data [33]. Li *et al.* [34] observed that turbulence effects were substantial in reducing the achievable resolution in azimuth and elevation at long range (8.2 Km) using a single-photon system, especially during the day and in an urban environment. Pawlikowska *et al.* [35], [36], have performed an extensive study of the effects of turbulence on a photon counting system at 1550 nm using both single element and arrayed detectors, and Henrikson and Sjoberg [37] have investigated methods for correction of scintillation effects in laser radar systems. To model this theoretically on a single line of sight is complex; Huela *et al.* [38] progressed from simpler models for beam wandering and scintillation to more complex theory for phase front distortion, comparing their work with previous attempts. In summary, the effect of turbulence is very much dependent on atmospheric conditions, natural or man-made, but these works have been directed at much longer ranges than is common in an automotive environment, and are unlikely to be the major concern in this application.

B. Choice of Detector

For FWL, there are two main types of detector, linear mode avalanche photodiodes (APDs) and time-correlated single-photon counting (TCSPC), typically using Geiger mode APDs or single-photon avalanche diode (SPAD) detectors [39]. APDs operate in linear multiplication mode, where the output signal is linearly proportional to the incident optical power level, thus providing full waveform information. These systems have proven robust and reliable and have been used in a variety of long-range LiDAR applications, but typically require detection thresholds of the return signals of the order of several 100s photons [39]. Single-photon LiDAR systems use APDs biased above the avalanche breakdown voltage so that a single-photon can initiate a self-sustaining and readily detectable avalanche current. These detectors can register only the presence or absence of a photon and cannot distinguish between one or two (or more) photons incident at the same time. The advantage of the single-photon approach is sensitivity at the single-photon level, which when coupled with high repetition rate laser sources, can produce an FWL response over many laser cycles. The picosecond jitter of TCSPC systems can provide an advantage in terms of signal-to-noise ratio and, significantly, in terms of depth resolution (of the order of centimeters) when compared to linear mode detectors. These advantages have been apparent for a number of years [40], but have suffered from long data acquisition times, too slow for most automotive applications. However, as discussed in Section VI-A1, the development of detector arrays, allied to rapid image processing techniques [41], suggest that TCSPC LiDAR systems can become more effective for future automotive requirements.

When imaging through obscuring media, light is attenuated in both directions, so for a linear APD the return signal amplitude is greatly reduced and may be missed in the presence of system noise and back-scatter from the medium. In a TCSPC detection system, however, the detector can only trigger only once per laser pulse, with the detector requiring a reset after each event, typically resulting in a detector dead time of 10's nanoseconds. If the likelihood of photon returns is high compared to the pulse rate then a statistical skew in measurement probability will occur across the timing window, called pulse pile-up. This pile-up effect will be of particular significance in multiple return measurements through adverse media [28], [39]. In previous work, the authors have corrected single photon returns for loss of light through vegetative layers [42], but this does not fully correct for pulse pile up effects. In short, if TCSPC is to be used for full dynamic range depth imaging in the automotive context, rather than applying a window with limited depth of field ('gating'), further statistical correction is needed.

C. A Comparison With Automotive Radar

Automotive radar has the particular strengths of relatively long range operation, is unaffected by lighting conditions (e.g. at night) and is less sensitive than optical sensors to obscuring media such as rain, mist, smoke or fog. Unfortunately, current azimuthal and elevation resolution of automotive radars is poor, and this makes detailed scene mapping and object classification challenging and error prone. Automotive radar imaging and processing systems [10] are generally targeted at the millimeter-wave region from 30–300 GHz (1 cm to 1 mm wavelength),

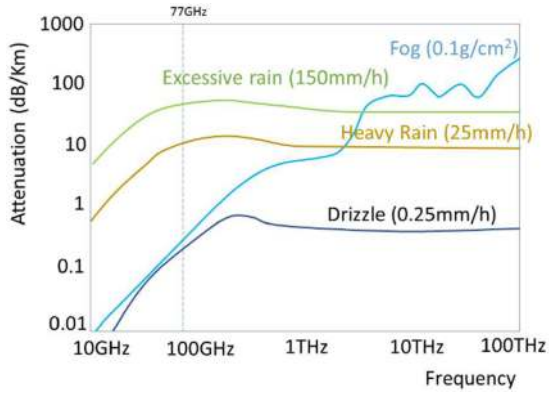

Fig. 6. Absorption spectra in fog and rain, from [45], [46] (©2012 IEEE).

penetrating poor weather [43] and receiving echoes from both surfaces and actors within the field of view and at medium to long range. 77 GHz is a popular choice, but increasing frequency and modulating bandwidth in an FM system improves depth resolution, shown by experiment for a 150 GHz FMCW radar [11]. In comparison with LiDAR, radar signals can propagate through dense obscurants such as fog with much smaller propagation loss [44], but the greater impediment to detailed scene mapping and actor recognition is the low azimuth and elevation resolution due to beam spread.

However, examining Fig. 6 one can observe that relative to fog, in rain there is much higher attenuation [45], [46]. In an explicit study of the effects of adverse weather on automotive radar, Zhang *et al.* [47] note that rain, snow, mist, and hail, can all have a significant impact, showing for example how the received power and probabilities of detection of vehicles and pedestrians reduce considerably as rain density increases. Noruzian *et al.* [48] measured experimentally the effects of snowfall, concluding that as the density of snow increases, so the attenuation increases at all measured wavelengths. Comparing wet and dry snow, higher attenuation occurred in the former case.

In experiments to compare current automotive optical imaging and a prototype automotive radar [49], a marquee was filled with artificial (glycol based) obscurant and images were taken using a 150 GHz FMCW azimuth scanning radar, a Velodyne HDL-32E LiDAR and a StereoLabs ZED optical stereo camera. In Figs. 7 and 8 the radar image can be compared against clear optical images and against optical images acquired at a visibility of 4.4 m, as measured by a Secchi disc. At shorter distances, the radar image shown in Fig. 7 is unaffected, but if we examine the optical stereo image it is difficult to discertain the highlighted objects, and several LiDAR returns at the further distances are not detected by the algorithms used in the Velodyne system. This illustrates very clearly the need for sensitive, full waveform processing as argued in this paper.

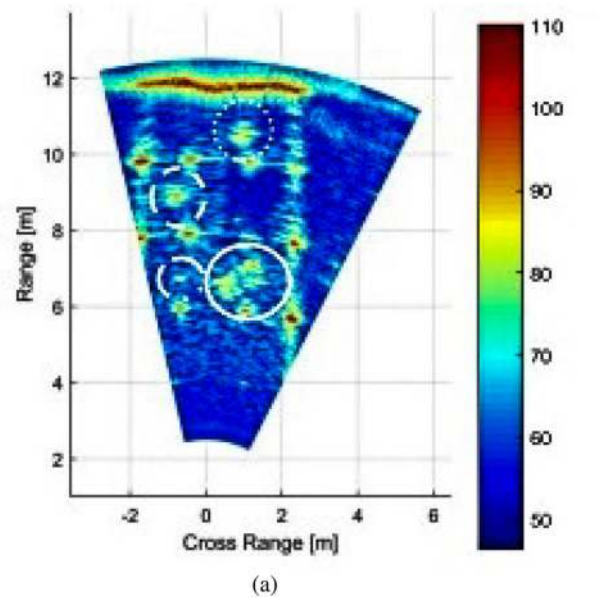

(a)

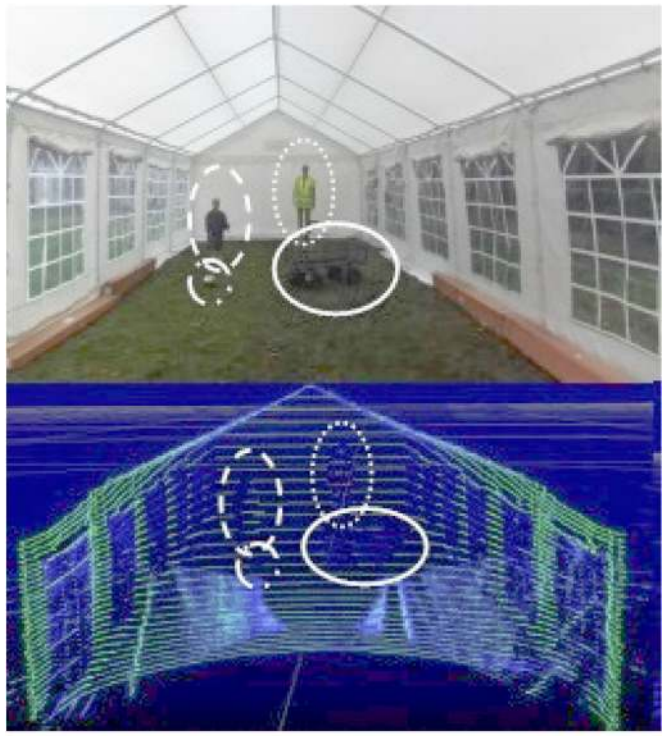

(b)

Fig. 7. Scene within tent before smoke machine is switched on, from [49]. The ellipses enclose two mannequins, a spherical target of 20 cm diameter (on the left) and a trolley (on the right). From top to bottom are the radar, camera and LiDAR images. (©2017 IET). (a) Radar Image. (b) Optical Stereo (Left) and LiDAR Images.

D. Fusion

As introduced in Section I, given the complementary strengths of the different sensors [50], all prototype vehicles for autonomous and assisted driving have sensor suites designed to cope with the different conditions. However, most sensor fusion methodologies [3] rely on unchanging descriptions of prior and error probabilities that are not appropriate to changing weather conditions. For example, RobustSENSE [51] employs {LiDAR, stereo camera, short and long range radar} sensors for external environmental monitoring, aiming to maximize sensor performance while keeping component costs reasonable ($\leq$1000

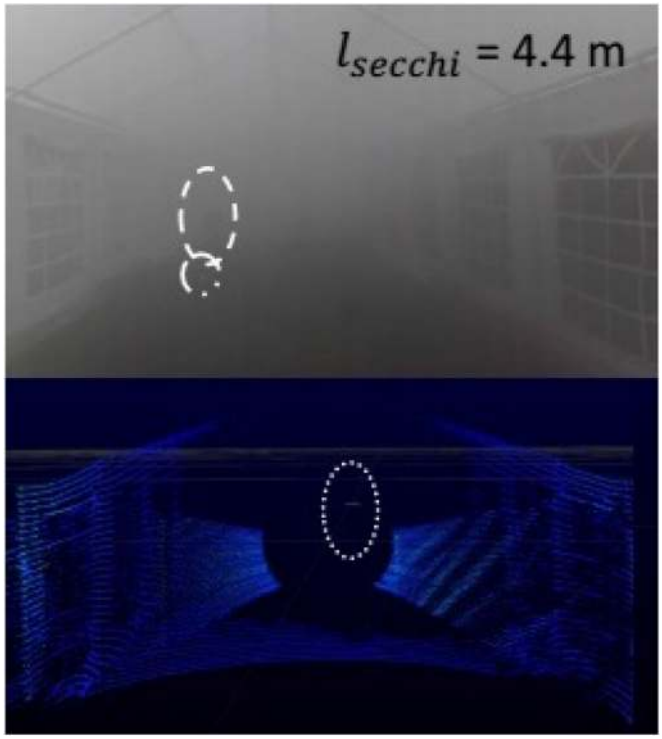

Fig. 8. Scene within tent as smoke density increases to give 4.4 m visibility [49]. The camera and LiDAR images are shown. (©2017 IET).

Euro). Radecki *et al.* [16] present algorithms for data association, object tracking, and object classification using video, LiDAR and radar, detecting and tracking cars and pedestrians in a variety of conditions, {Sunny, Night, Wet and Cloudy, Snow, Rain}. In addition to attenuation and image distortion, they paid attention to sensor fouling in snow, rain, and dusty conditions, and gave a full discussion of how these effects occur and how to avoid the associated problems. For fusion, one needs a switching strategy, and variable parameters according to conditions. Trivially, this could be optical in good weather, radar in bad weather, but this suggests we need algorithms to determine when to switch, touched upon in Section III-E.

E. Online Fog Determination

If fog (or other weather) is an impediment to optical imaging because it attenuates and degrades the recorded image, the corollary is that measurements of passive optical and LiDAR image data can be used to estimate fog or other pollutant densities [45]. Pfennigbauer *et al.* [22] suggested that it was possible to determine the visibility range and hence estimate fog density from a LiDAR waveform measured from immediately in front of the sensor to a maximum range of 30 m, since the rate of amplitude decay was a clear indication of this. This suggests a way to recover targets hidden in fog, because if the distributed return from the relatively homogeneous fog can be measured, this can be substituted in a model that analyzes multiple real target echoes against a known background [52], [28].

As a rare exception, Shamsudin *et al.* [53] have investigated algorithms for fog detection and elimination from 3D point clouds and conducted experiments under laboratory conditions. This uses intensity and geometrical distribution to separate clusters and is applied to the much more constrained situation of an indoor robot. Effectively, it is an outlier removal algorithm based on geometry, laser intensity and the beam itself. This is unlikely to be robust outdoors over wide range fields as beam divergence, different surface reflectance and distributed surfaces all confuse the issue.

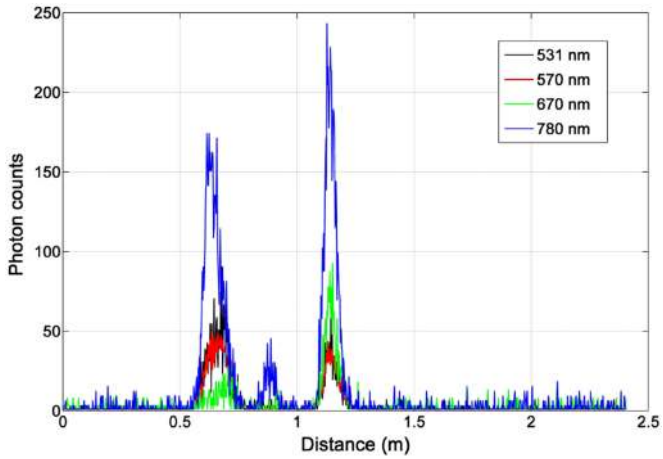

Fig. 9. Multispectral data for a single pixel through tree canopy, from [42]. In this case the stand-off distance was 45 m to the zero reference point, just above the tree apex. (©2014 IEEE).

IV. Full Waveform LiDAR Signal Analysis

Current automotive LiDAR systems [5], [6] work on single or occasionally dual peak detection, using a constant false alarm rate (CFAR) matched filter or a similar strategy, assuming that return signals from the LiDAR are significantly above a constant noise floor. We consider temporal pulse modeling of a FWL return as a non-normalized statistical mixture of single surface returns rather than as an aggregated convolution. Such a waveform has density $F(i;k,\phi)$ [54] defined as

$$F(i;k,\phi) = \sum_{j=1}^{k} f_{\text{system}}(i;\beta_j,t_{0_j}) + B \tag{1}$$

where k denotes the number of returns, β each peak amplitude, t_0 peak position, and B the background. Examples of four such waveforms for a single array pixel are shown in Fig. 9.

FWL processing to extract the parameters of Equation 1, as surveyed by Mallet and Bretar [55], is the key to extracting meaningful information from more complex scenes in which the simple model of reflection from a single (or possibly dual) flat surface with negligible depth variation normal to the beam direction, as used for example in the Velodyne scanner [56], is not appropriate. Multiple echoes can occur due to secondary reflections [57], imaging from and through transparent surfaces [58], [59], imaging through complex surface structures with mean size less than the beam width such as trees [42], and of particular relevance to the automotive case, through obscuring

media in which much of the return is scattered from particles between the sensor and objects of interest, shown in Fig. 5.

Wagner *et al.* [13], following [60], [61], considered the returned signal as a mixture of Gaussians. In the system considered, pulses were wide, of the order of 5 ns, corresponding to 1.5 m distance, so resolution of closely separated surfaces was difficult. Rather than resolve, Mallet *et al.* [62] considered the waveform as a distributed response characteristic of the target, using a similar pulse width and a large footprint, of the order of 25 m^2. A set of characteristic signal return models (generalised Gaussian, Nakagami, Burr) was used to discriminate between cathedrals, lesser buildings, grass, fields and streets. However, an automotive LiDAR operates at shorter range, less than 200 m. If we employ a narrow pulse and beam width in a time correlated photon counting (TCSPC) LiDAR system [40], the footprint on an opaque surface is much narrower, and the change in pulse shape due to surface variation in azimuth and elevation is negligible. This means we can build a high resolution image by scanning or a focal plane array.

Several strategies have been proposed to estimate multi-peak parameters given the observed photon histograms. The key advantages of a Reversible Jump Markov Chain Monte Carlo (RJMCMC) approach [52], [63], following [64] are the ability to detect very weak and closely based returns, as short as 1 cm at a distance of 330 m [52], but these algorithms are time-consuming. Other algorithms [59], [65], [66] consider a convex formulation coupled with sparsity promoting regularisation. These approaches take into account the Poisson statistics of the data and use optimization and employ assumed spatial correlation between pixels. This latter constraint can be used to discourage adjacent pixels from having different values of k (number of peaks) [67], enforce neighbouring pixels to share similar depth and reflectivity estimates [41], [68], [69], or even account for non-local spatial correlations [63], [70]–[72]. These algorithms have been demonstrated on real data showing considerable performance improvements; examples of their use in real studies of object perception through fog are provided in Section V-B.

V. Experimental Studies on 3D Imaging Using TCSPC Data Through Obscuring Media

We now report our own, and other studies, on 3D image formation using FWL through various obscuring media and extrapolate to the automotive case. As discussed in Section III-B, for much published work and for existing commercial systems the preferred receiver technology is usually based on the Avalanche Photodiode (APD). In our experiments, we employed Time-Correlated Single-Photon Counting (TCSPC) with excellent sensitivity, depth resolution, and operated at eye safe low laser power, all advantageous for automotive applications.

A. Penetrative LiDAR Through Tree Canopies

We investigated multispectral LiDAR imaging of forest canopies to the ground floor along the tree apex direction (e.g. from the perspective of an airplane) [42]. The obscuring media is the canopy, so we can perform penetrative analysis, e.g. to determine the presence of invasive species on the ground. Equally, the canopy itself is of interest and using multispectral FWL we recovered parameters to infer structural and physiological processes.

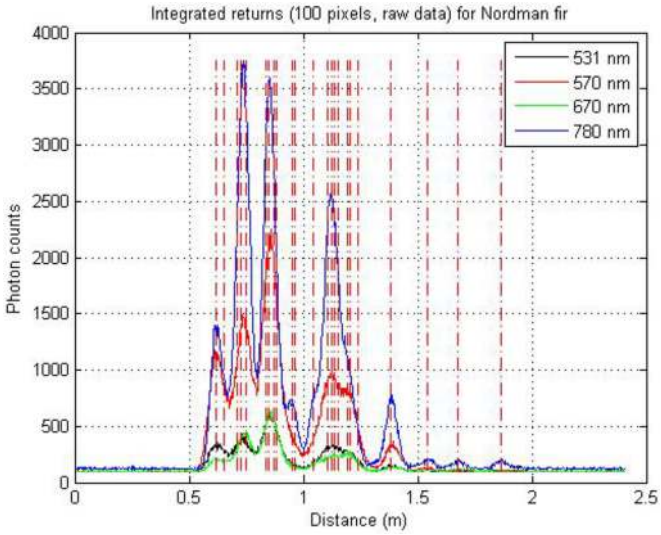

Fig. 10. Multispectral Data for 100 accumulated pixels through the tree canopy, from [42]. (©2014 IEEE).

In field trials, we collected a 10 by 10 matrix of full waveform data from a viewpoint normal to the apex of a small conifer. Fig. 9 shows the pixel illuminated by four independent wavelengths (531 nm, 579 nm, 670 nm and 780 nm). Fig. 10 shows the response for these same four wavelengths integrated over all the pixels, which is analogous to a wide footprint aerial sensor. As stated previously, some have used an aggregated model to represent the obscuring medium, such as generalised Gaussian, Nakagami, Burr functions to represent the tree canopy [62], or a gamma function to represent homogeneous fog [28]. Using RJMCMC analysis, supplemented by additional parameters to define spectral response, we recovered the relative abundance of needle and bark through the canopy, as well as the ground surface and height of the tree, using the model of Equation (1) with an unknown number (k) of impulse responses. The dotted lines in Fig. 10 are effectively the positions of instrumental returns and show the recovered positions of several layers of the tree canopy, and the ground, and each layer has a corresponding area and reflectance model, leading to the abundance recovery. Like Fig. 5, the last return is of low amplitude because the tree crown is relatively dense, so that little radiation penetrates to ground level. Fig. 10 shows that the bulk of the canopy returns are between approximately 0.6 m and 1.5 m, and the ground plane return is at approximately 1.8 m, and that although the vast majority of the photon returns are for the intervening medium (the canopy), there is nevertheless sufficient return to recover the "'target"' depth, assuming that the ground height is the parameter of interest. The key lesson for automotive LiDAR is that where multiple surfaces may exist within the fog, or the fog is itself non-homogeneous, the superposition of impulses allows a more

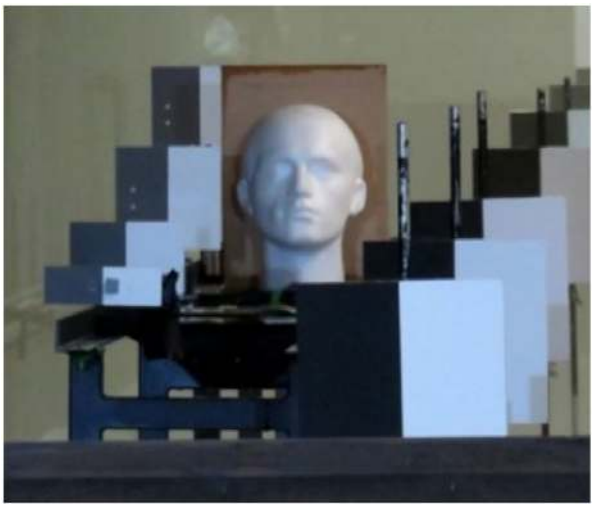

Fig. 11. Polystyrene head and calibration targets used in France for 3D imaging work through obscuring media, from [27]. (©2019 IEEE).

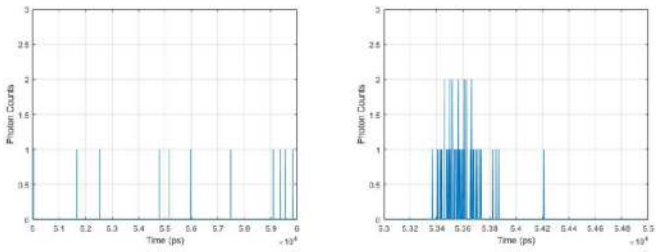

Fig. 12. Examples of photon count histograms under different levels of attenuation. These are focussed on a narrow time (distance) window of 2000 ps (30 cm) extracted from the full measurement window of 65536 ps (9.8 m) [27]. (a) 14:00 hours. (b) 14:55 hours.

flexible model than predefined aggregated distributions [28], [62].

B. Penetrative LiDAR Through Smoke and Fog

We now turn our attention to a more detailed study of LiDAR imaging through obscurants (smoke, fog) conducted in a sealed tunnel using different media and densities of the intervening medium [29], a situation which is more representative of the automotive case. For our experiments, we used a polystyrene head and a series of planar targets, as shown in Fig. 11. The transceiver was located at a stand-off distance of 17 m from the tunnel, and the head at a distance of 24 m from the tunnel entrance so that the total transceiver-target stand-off was 41 m. In Fig. 12 are shown a single pixel captured as the tunnel is filled with smoke (14:00 hours) then the corresponding pixel image after most of the smoke has dispersed (14:55 hours). These measurements are *gated around the target*, unlike Fig. 5, but there is no clear concentration of photons at the object surface in Fig. 12(a) due to reflections from the surrounding fog.

Satat *et al.* [28] have also recovered dense depth images of mannequins, similar in essence to those shown in Figs. 11 and 5, through fog in a specially constructed chamber. Like [62], they applied the alternative approach to the superimposition of

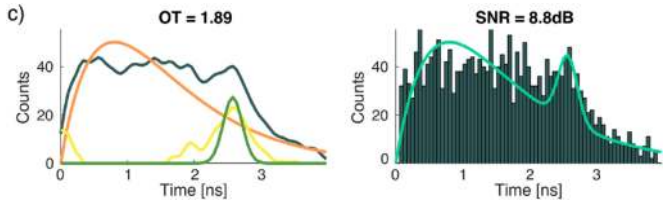

Fig. 13. An example histogram from [28]. OT refers to the optical thickness of the fog. On the left the orange curve is the fitted Gamma function, and the green curve is the assumed surface return. The yellow function denotes the difference. (©2018 IEEE).

a variable number of impulse returns which is to model the obscuring medium by a representative gamma function convolved with the instrumental response, as shown in Fig. 13. A Kernel Density Estimate (KDE) smooths the original signal, then the fitted gamma function at a given optical thickness (OT) is subtracted from this to leave the signal estimate, and the assumed single surface return is extracted. The key problem here is the assumption of a single return so that peaks in the yellow signal are assumed to be inhomogeneities in the fog rather than real surface returns.

In a scene such as this, it is possible to incorporate assumptions about the nature of the objects depicted, in particular the smoothness of the surfaces with few significant obscuring or sharp curvature edges. In Fig. 14 are shown several examples of reconstruction of the depth image of the polystyrene head that take advantage of either local or non-local spatial constraints, in addition to data statistics. In particular, the paper by Tobin *et al.* [27] compares Multidimensional Nonlocal Reconstruction of 3D (M-NR3D) [27] against two earlier approaches, Restoration of Depth and Intensity using Total Variation (RDI-TV) [73] and the Unmixing Algorithm (UA) [68]. The regularization term included variation in intensity as well as depth, as both the head and planar surfaces are of uniform Lambertian reflectance. In more complex scenes it may be more appropriate to regularize based on consistency of normal or curvature data or on the assumption of a few piecewise extended surfaces [74], [75] but this may make an already time-consuming optimization strategy intractable as we consider in Section VI.

In similar vein, we also recorded spectral transmittance at wavelengths from $500-900$ nm for different sediment densities in sea water in comparison with clear water, from both single-pixel scanning [76] and arrayed detector [77] configurations. Like the tree canopy examples, FWL processing was used to compute the peak positions, amplitudes and background photon count, and to classify target objects (model mines) through underwater vegetation [78]. In essence propagation through underwater sediment is analogous to propagation though airborne obscurants and is not considered further here as it does not add to the discussion.

VI. Complexity: Hardware and Software Issues

Complexity issues are key in dealing with the much greater volume of data associated with FWL. We have to be system-centric, considering focal plane vs. scanned hardware, how data

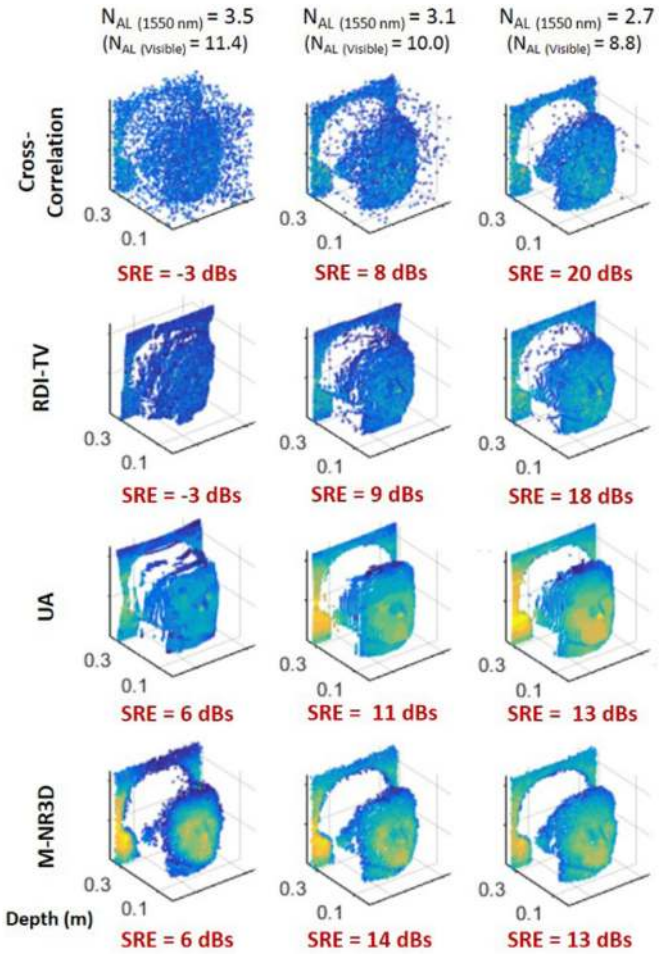

Fig. 14. Depth image restored by a number of methods using spatial constraints and data statistics. N_{AL} is number of attenuation lengths in glycol based smoke. The per-pixel acquisition time was 3 ms (approximately 30 seconds total). The data was reconstructed using, from top to bottom, cross-correlation; RDI-TV [73]; UA [68]; M-NR3D [27]. The depth scale is in meters for all images.

is acquired and read out, where and how it is processed, and what computational languages and hardware are most appropriate. In Section IV we argued that FWL required sophisticated techniques to recover weak and closely separated returns expected in imaging complex scenes through obscuring media. Methods such as RJMCMC or the convex optimisation methods have significant time complexity. In brief, to achieve high frame rate processing, especially in the presence of obscurants, requires significant progress in sensor design, algorithms, software and embedded hardware.

1) Solid State Arrays: Solid state detector arrays: Over the last few decades, silicon-based SPAD arrays have come to prominence for a variety of applications, particularly when fabricated in CMOS technology [79]. These sensors have been configured in full TCSPC mode [80], [81], and for single-photon 3D imaging in range-gated mode [82], [83]. Over the years, there have been considerable developments aimed at improving the fill factor, the quantum efficiency, reducing crosstalk, and incorporating fast read out circuitry [81], [84], [85]. Arrayed silicon SPAD detectors are being developed explicitly for the automotive sector [5], with detection capability demonstrated at up to 300 m. Larger arrays are now being fabricated, e.g. of 256×256 [86] or 252×144 pixels [87]. Earlier [88], a 64×32 pixel array was operated at an even higher rate of 100fps. More recently, Gyongy *et al.* [89] demonstrated 1000fps depth imaging using a 80×30 SPAD array with TCSPC capability having an on-chip histogramming capability.

With silicon-based SPADs, the spectral range is limited to wavelengths below 1000 nm. As highlighted in Section III, there are advantages in using longer wavelengths. Up to approximately 1600 nm, this has been addressed by the use of InGaAs/InP and InGaAsAsP/InP SPAD detectors [83], [90]. Itzler at al [90] demonstrated these picosecond-resolution TCSPC-based detector arrays in formats of 32×32 and 128×32 pixels applied to many applications including: high speed depth profiling at 1000fps [91], panoramic 3D profiling in clutter [92], and real-time depth reconstruction of complex, multi-surface scenes [41]. Pawlikowska [35] provides a thorough account of the relative merits of a scanned, single element 3D InGaAs/InP TCSPC LiDAR system against a non-scanning transceiver system containing a 32×32 InGaAs/InP SPAD detector array.

However, all of these process the data on the basis of an assumed single surface return to limit complexity. Of concern is the need to achieve high resolution over the full dynamic range, typically 4 cm resolution from 1–200 m in the automotive case, which places very high demands on data storage and processing in an array structure. If using a focal plane array, there are limited space and thermal budgets, and if we increase the complexity of the data storage (e.g. for full histograms instead of single points), then we reduce the fill factor and the frame rate accordingly [93]. Simple binary logic and external frame summation can reduce the frame time (to as low as 10 ms [94]) but that does not allow full wave data analysis of the type described in Section IV. To achieve FWL LiDAR data comparable to video resolution in azimuth and elevation would require in excess of 10^9 measurements per frame, which is unachievable now, and so current, commercial sensors [5], [6], [22] process single echoes at low vertical resolution, or multiple echoes on single elevation sweeps, relying on sensor movement to 'pushbroom' the remaining dimension.

2) Array Architectures and Compressed Sensing: As stated in the previous paragraph, in addition to maintaining high detection efficiency and fill factor in a high resolution integrated sensor, for FWL we have to store, transfer and process long data vectors at each pixel, i.e. the depth profile, e.g. in contrast to the triple RGB values recorded by a camera. This puts a premium on space and thermal budgets, so full sensors generally have low resolution in all spatial dimensions, and if processing is integrated then it has to be very simple, e.g. a centre of mass computation on the response. To try and resolve this and eliminate the need to process every pixel, the first applications of compressed sensing technology, e.g. [95], [96], were applied to single pixel cameras, random sampling from a dense pixel matrix using a digital-micro-mirror-device (DMD) to provide the data to reconstruct 3D surfaces on the assumption of few smooth surfaces, and in some cases uniformity of reflectance as well.

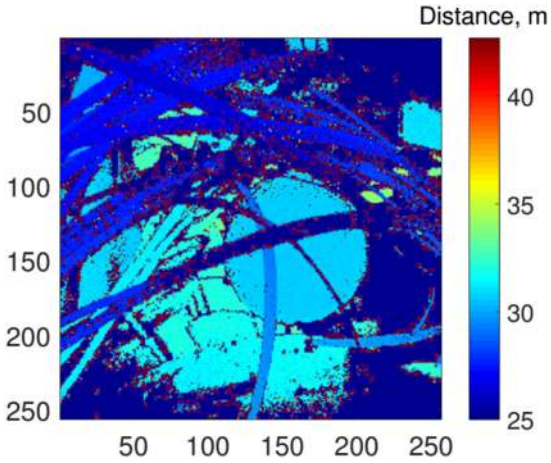

Fig. 15. Reconstructed scene from compressed reconstruction at a frame processing time of 1 ms, from [97]. The scene is complicated, with several surfaces separated by sharp, blade edges, and as such is representative of the kind of data expected in the automotive context. (©2019 IEEE).

Recently, we expanded the CS methodology [97] into a programmable array, synchronizing the receiver and transmitter, boosting the signal-to-noise-ratio (SNR) by restricting active measurements to the patterns constituting the sensing matrix. To reconstruct depth in the CS framework, a mixed domain approach was adopted and simplified, using total variation (TV). Earlier work relied on iterative processes to find the sparsest solution and were computationally expensive for images larger than 64×64 pixels [95], [96]. In contrast, we sampled and processed the scene in small individual square tiles. The algorithm was encoded in Matlab to reconstruct 3D scenes using full waveforms derived from both synthetic 64×64 [98] and real 256×256 data [78]. An example of a reconstructed scene is shown in Fig. 15. The key observation is how the application of full waveform, compressed sensing, implemented on a GPU reduces the frame processing times to below 10 ms, which is comparable to the necessary frame rates for the automotive area.

3) Reducing Algorithmic Processing Time: For deployment in automotive scenarios, it is essential to reduce the computational cost of existing algorithms. Assuming a preferred algorithm, the necessary first step is to profile the code. Quantifying the performance of RJMCMC processing in comparison with the prevalent less complex approaches [99] showed that simple likelihood computation accounted for 90% of the processing time. This can be accelerated by special purpose hardware.

Improving data representation is important. For example, working in sparse regimes requires the use of a photon tagged representation [63], [68], but in dense regimes it is more efficient to work with FWL histograms in the presence of a scattering environment [100]. Simplifying assumptions, if valid, also ensure faster performance. This can include fixing the number of estimated peaks, the use of down-sampled data to reduce dimensions and proposing specific formulations that allow parallel and GPU computing tools. For example, in [101] we examined the ability to resolve closely spaced surface returns, one of the key strengths of TCSPC FWL systems, with a much faster approach. The

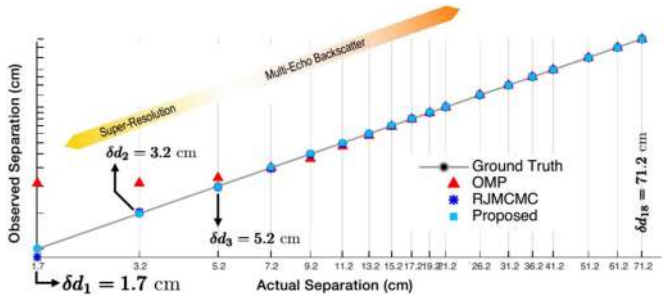

Fig. 16. Measurement of surface resolution using the RJMCMC, OMP and the Matrix Pencil methods from [101]. The Matrix Pencil method results in a reduction of per pixel processing time from 1s to 1.8 ms. (©2016 IEEE).

problem was reformulated as a parameter estimation problem pivoted around the finite rate of innovation framework [102]. As shown in Fig. 16 [101] we were able to achieve similar results to full RJMCMC [52], but in a fraction of the time, reducing computation time per pixel from 1s to 1.8 ms per pixel. This comes with the caveat that it relies on low pass filtering of the raw data, and on an a-priori assumption of two, relatively strong returns. However, this approach does not make any a-priori assumptions on spatial constraints, as in Fig. 14, so in that sense is more generally applicable.

4) Parallel Methods for Full Waveform Analysis: If we consider single pixels, or pixel windows, then the simplest form of data parallelism is to process these independently and in designing new arrayed sensors this can be encapsulated in on-chip processing. As the same instruction sequence is performed on multiple data sets, this makes it suitable for implementation on a single-instruction-multiple-data architecture, such as the new range of GPUs.

In [103], we also looked at multiple-instruction-multiple data (MIMD) methods to implement the RJMCMC methodology, using both control and data parallelism. This facilitates concurrent sampling by forming a group of parallel chains, decomposing the state space into subsets of parameter space. The complete state space of n candidate models, $\{k_1, k_2, \ldots, k_n\}$ is divided into $(n - m + 1)$ groups, each containing m adjacent models, i.e. $\text{group}_i = (k_i, k_{i+1}, \ldots, k_{i+m-1})$. Each group is assigned an independent RJMCMC chain, hence reducing the between-model mixing complexity by reconfiguring the state space. An implementation on a 32-node Beowulf cluster led to significant speedup, of the order of 15–25 times, while maintaining the same capability of RJMCMC to better explore the whole solution space having several possible echoes.

VII. Conclusion

We have addressed some of the key strengths of full waveform LiDAR (FWL) with particular regard to obscuring media. We aim to prompt a discussion on the key strengths and weaknesses for deployment of FWL to allow autonomous or driver assisted vehicles to operate in adverse weather, including smoke, fog, mist and precipitation. Although we focus on automotive LiDAR, by which we assume cars and public transport used by the general population, such discussion encompasses more

specialized applications, such as emergency vehicles operating in adverse conditions, e.g. during fog that causes an accident, or sensor controlled robots operating in extreme environments, e.g. underground or in a smoke filled building. We now summarise the main issues.

There is the issue of *operating range*, even in good weather. Photon counting LiDARS have high sensitivity, and combined with new developments in sparse modeling of scenes and very efficient scanning optics have been shown to work at long ranges [35], [104] but these are not (yet) suitable for automotive applications. In addition to issues of optical and computational efficiency, in general, the 3D reconstruction algorithms make simplifying assumptions, e.g. that 'reflectors are clustered in depth' [104], so that many pixels can be aggregated, which is questionable in an automotive context. In contrast, current automotive LiDAR manufacturers claim ranges in excess of 100 m; in our own experience even this is dependent on good reflectivity and favourable ambient light. A move towards the 1550 nm wavelength should increase the operating range while remaining within laser eye safety thresholds. In some adverse conditions, such as dense smoke, the attenuation is also reduced at the longer wavelength, so again this would improve operating range. However, the move to 1550 nm wavelength comes at a cost when compared to silicon where there is a considerable legacy of materials and device optimisation. Single-photon detectors are now being developed for wavelengths around 1550 nm using Ge-on-Si [105], [106] which may reduce costs if markets stimulate mass production.

Many existing automotive LiDARS use single return, or perhaps dual (e.g. strongest, last) return only processing. If FWL and TCSPC technology can be applied this will allow not only improved *distance resolution* but also the capability to detect and characteristic weak returns. Single shot *image plane resolution* is usually poor. Scanning systems give dense spatial sampling in the spin direction but generally use sparse sampling normal to the spin direction, e,g, 32–128 lines, so that denser sampling requires vehicle movement. If the spin rate is fast and vehicle movement can be accurately monitored, and point clouds accurately registered, then this may suffice. On the other hand focal plane arrays have generally many fewer pixels than conventional CCD cameras, so either larger arrays must be developed, or mosaics of smaller sensors configured. The array fill factors are also improving [81], [85], which together with micro-lensing [84] should allow a more dense sampling of the scene.

There are *storage and processing* issues for FWL. In the penetrative LiDAR studies cited above, a sensor acquires a full waveform at each pixel or scan direction; this is then processed to find the multiple reflections contained therein. To store and read out such voluminous data at each pixel requires additional circuitry that reduces the semiconductor area available for sensing, and also takes considerable time, reducing frame rate. Conversely, to introduce on-chip processing using other than simple centre of mass detectors, would be both area and time expensive. Having said that, there may not be a need to store then post-process full waveform data. Taking TCSPC sensors as an example, one can consider each photon arrival as an event that updates range estimates, which are retained as new photons arrive.

A number of authors have shown that *compressed sensing* [107] has the potential to acquire high resolution images from relatively few samples, usually sampled at random [63], [65], [95]. The advantage of reducing the number of pixel samples, and using optical methods to sample randomly, is that it allows us to use fewer pixel sites and attain faster frame rates. Further, it can potentially release sensor area for readout and processing circuitry. However there are some caveats. Compressed sensing relies on the signal or image being sparse in some domain, and the majority of illustrations of compressively sensed LiDAR use simple test scenes with simple surfaces and even uniform reflectance. Further, success is often measured by a reconstructed distance from ground truth, which is best on continuous surfaces rather than significant blade or fold boundaries. In an automotive LiDAR, the anomalies have precedence over the common-place, so one has to be careful that the sparse domain does not eliminate the irregularities. Equally, in scene reconstruction it is important to be sure that the underlying sparsity assumptions are applicable, and to include estimates of uncertainty on the reconstructed scene data. Nevertheless, the concept is promising for future automotive systems.

Allied to the potential of compressed sensing, there is a key requirement for *algorithmic acceleration*. Much has been made of the recent, ubiquitous application of deep learning, but the recent progress is due in large part to hardware innovation such as relatively low cost GPU architectures. So there is a requirement for stack (task $->$ algorithm $->$ code $->$ compilation $->$ hardware) analysis of solutions to the signal and image analysis problems presented here, including for example delegation of repetitive maths to FPGAs, application of SIMD and multi-core architectures as appropriate to the problem, as shown in Section VI

In Section V we presented a number of examples of penetrative LiDAR in action. In some of these studies the target was gated so the surface shape was sensed using a-priori knowledge of distance, i.e. using differential depth of focus. However, in an automotive LiDAR, the assumption is that the scene must be sensed at all ranges, and in adverse weather, one must *analyse the medium*. This was best illustrated by the tree canopy example [42], but if we examine sensing through fog, we realise we cannot assume a homogenous and constant arrival of returned light as a function of depth, as is the case in almost all previous research. Allied to this, in an automotive system, if we want to adjust dynamically to changing conditions, then we need to know what those conditions are, a circular problem.

Hence, although LiDAR research and development is proceeding apace, is it likely in the short term that this could become a sole sensor of choice? It seems that in the near term at least *sensor fusion* [3] will remain necessary. For example, radar is well know to operate well in bad weather but suffers from poor scene resolution, currently a focus of improvement using different radar frequencies, and processing methods such as Doppler beam sharpening and synthetic aperture. There is also variability on return that leads to difficulty in target recognition or detection in cluttered environments (by which we mean

having several confusing objects such as echoes, potholes, line markings, which are difficult to model in electromagnetic simulation, rather than statistically modelled background). Similarly, we know that video processing for object recognition is much more advanced, but both this and stereo scene reconstruction suffer badly in adverse conditions. Therefore, we would suggest that FWL filtered by better resolved radar data to give a-priori information about coarse scene structure, could in future give highly resolved scene reconstruction, but not immediately.

Less studied, *interference* or *crosstalk* [9] between different sensors operating in a cluttered environment such as a road network is a potential problem. In terms of ambient light, a scanning LiDAR employs spatial (through a directional beam), spectral (using a narrow band filter) and temporal (gated range) filtering. Yet, Carballo *et al.* [30] found considerable interference between multiple LiDARS in a weather tunnel, in the form of both fringe patterns and random echoes, but were unable to model these effects theoretically. Most models that do exist, e.g. [108], are based on solution of the laser radar equation with a realistic automotive or other transceiver model, and either a synthetic environment or a mathematical model of probability of return. Hence, automotive LiDARs should have some degree of immunity to ambient effects, even in strong sunlight. If a focal plane array is used, with a wide footprint transmitter for parallel data acquisition, some capability for spatial filtering is lost. As the dynamic range must be over 100 m or more, this negates a degree of temporal filtering. Therefore, most authors suggest that some further form of sensor specific modulation, e.g. code division multiple access [25], is required to disambiguate the intended from other sources. Again, this is really designed for single returns, as multiple surfaces will alter the received code, and the effect of an obscurant is to provide many such additional returns. To the best of our knowledge, models and coding strategies for avoiding interference using FWL in obscurants have not been addressed.

Finally, there are *design and cost* concerns. Whereas one can buy a CCD camera or a car radar for less than $200, LiDAR systems are comparatively expensive. Further, it is not practical to have a scanning LiDAR or indeed radar system mounted on top of a production vehicle. Hence, the future of full waveform LiDAR rests on the design of focal plane arrays, with or without compressed sensing, that satisfy all the requirements of the previous paragraphs in this section. If and when such technology becomes ubiquitous, then the cost per installed system should drop considerably.

In conclusion, we would suggest that FWL is a key component of future sensing systems for the automotive sector, and in the face of adverse weather conditions, analysis of the intervening medium is a crucial component of the development of algorithms and sensors.

REFERENCES

[1] J. Guerrero-Ibez, S. Zeadally, and J. Contreras-Castillo, "Sensor technologies for intelligent transportation systems," *Sensors*, vol. 18, pp. 1–24, 2018.

[2] N.-E. E. Faouzi, H. Leung, and A. Kurian, "Data fusion in intelligent transportation systems: Progress and challenges: A survey," *Inf. Fusion*, vol. 12, pp. 4–10, 2011.

[3] B. Khaleghi, A. Khamisa, F. Karray, and S. Razavi, "Multisensor data fusion: A review of the state-of-the-art," *Inf. Fusion*, vol. 14, no. 1, pp. 28–44, 2013.

[4] F. Alam, R. Mehmood, I. Katib, N. Albogami, and A. Albeshri, "Data fusion and IoT for smart ubiquitous environments: A survey," *IEEE Access*, vol. 5, pp. 9533–9554, 2017.

[5] J. Hecht, "LiDAR for self-driving cars," *Opt. Photon. News*, vol. 1, pp. 27–33, 2018.

[6] J. Halker and H. Barth, "LiDAR as a key technology for automated and autonomous driving," *ATZ Worldwide*, vol. 1, pp. 70–73, 2018.

[7] [Online]. Available: http://www.cvlibs.net/datasets/kitti/eval_3dobject.php. Accessed on: Apr. 18, 2020.

[8] I. Maksymova, C. Steger, and D. Druml, "Review of LiDAR sensor data acquisition and compression for automotive applications," *MDPI Proc.*, vol. 2, pp. 852–855, 2018.

[9] P. Angskog, P. Nasman, and L.-G. Mattson, "Resilience to intentional electromagnetic interference is required for connected autonomous vehicles," *IEEE Trans. Electromagn. Compat.*, vol. 61, no. 5, pp. 1552–1559, Oct. 2019.

[10] S. Patole, M. Torlak, D. Wang, and M. Ali, "Automotive radars: A review of signal processing techniques," *IEEE Signal Process. Mag.*, vol. 34, no. 2, pp. 22–35, Mar. 2017.

[11] D. Jasteh, E. Hoare, M. Cherniakov, and M. Gashinova, "Experimental low-terahertz radar image analysis for automotive terrain sensing," *IEEE Geosci. Remote Sens. Lett.*, vol. 13, no. 4, pp. 490–494, Mar. 2016.

[12] S. Gishkori and B. Mulgrew, "Azimuth enhancement for automotive SAR imaging," in *Proc. Int. Conf. Radar*, 2018, pp. 1–5.

[13] W. W. Wagner, A. Ullrich, V. Ducic, T. Melzer, and N. Studnick, "Gaussian decomposition and calibration of a novel small-footprint full-waveform digitising airborne laser scanner," *ISPRS J. Photogrammetry Remote Sens.*, vol. 60, pp. 100–112, 2006.

[14] R. Rasshofer, M. Spies, and H. Spies, "Influences of weather phenomena on automotive laser radar systems," *Adv. Radio Sci.*, vol. 9, pp. 49–60, 2011.

[15] G. R. Osche and D. S. Young, "Imaging laser radar in the near and far infrared," *Proc. IEEE*, vol. 84, no. 2, pp. 103–124, Feb. 1996.

[16] P. Radecki, M. Campbell, and K. Matzen, "All weather perception: Joint data association, tracking, and classification for autonomous ground vehicles," *CoRR*, vol. abs/1605.02196, 2016, *arXiv:1605.02196*.

[17] I. I. Kim, B. McArthur, and E. Korevaar, "Comparison of laser beam propagation at 785 nm and 1550 nm in fog and haze for optical wireless communications," in *Proc SPIE*, vol. 4214, pp. 26–37, 2001.

[18] F. Christnacher, B. Schertzer, M. N., E. Bacher, M. Laurenzis, and R. Habermacher, "Influence of gating and of the gate shape on the penetration capacity of range-gated active imaging in scattering environments," *Opt. Express*, vol. 23, no. 26, pp. 32 897–32 908, 2015.

[19] M. M. Ijaz, Z. Ghassemlooy, H. L. Minh, S. Rajbhandari, and J. Perez, "Analysis of fog and smoke attenuation in a free space optical communication link under controlled laboratory conditions," in *Proc. Int. Workshop Opt. Wireless Commun.*, Oct. 2012, pp. 1–3.

[20] M. Khan, S. Muhammad, M. Awan, M. Kvicera, V. Grabner, and E. Leitgeb, "Further results on fog modeling for terrestrial free-space optical links," *Opt. Eng.*, vol. 51, no. 3, pp. 1–10, 2012.

[21] X. Cao, P. Church, and J. Matheson, "Characterization of the opal LiDAR under controlled obscurant conditions," in *Proc. SPIE*, vol. 9839, May 2016, Art. no. 98390I.

[22] M. Pfennigbauer, C. Wolf, J. Weinkopf, and A. Ullrich, "Online waveform processing for demanding target situations," in *Proc. SPIE*, vol. 9080, 2014, Art. no. 90800J.

[23] M. Kutila, P. Pyyknen, H. Holzhter, M. Colomb, and P. Duthon, "Automotive LiDAR performance verification in fog and rain," in *Proc. 21st Int. Conf. Intell. Transp. Syst.*, 2018, pp. 1695–1701.

[24] M. Bijelic, T. Gruber, and W. Ritter, "A benchmark for LiDAR sensors in fog: Is detection breaking down?" in *Proc. IEEE Intell. Vehicles Symp.*, 2018, pp. 760–767.

[25] T. Fersch, A. Buhmann, A. Koelpin, and R. Weigel, "The influence of rain on small aperture LiDAR sensors," in *Proc. German Microw. Conf.*, Mar. 2016, pp. 84–87.

[26] M. Trierweiler, T. Peterseim, and C. Neumann, "Automotive LiDAR pollution detection system based on total internal reflection techniques," in *Proc. SPIE*, vol. 11302, 2020, Art. no. 1130216.

[27] R. Tobin, A. Halimi, A. McCarthy, M. Laurenzis, F. Christnacher, and G. S. Buller, "Three-dimensional single-photon imaging through obscurants," *Opt. Express*, vol. 27, no. 4, pp. 4590–4611, Feb. 2019.

[28] G. Satat, M. Tancik, and R. Raskar, "Towards photography through realistic fog," in *Proc. IEEE Int. Conf. Comput. Photography*, May 2018, pp. 1–10.

[29] R. Tobin, A. Halimi, A. McCarthy, M. Laurentzis, F. Christnacher, and G. Buller, "Depth imaging through obscurants using time-correlated single-photon counting," in *Proc. SPIE Conf. Adv. Photon Counting Techn. XII*, 2018, pp. 86–90.

[30] A. Carballo *et al.*, "Libre: The multiple 3D LiDAR dataset," 2020, *arXiV:2003.06129v1*.

[31] J. Zhao, Y. Li, B. Zhu, W. Deng, and B. Sun, "Method and applications of LiDAR modeling for virtual testing of intelligent vehicles," *IEEE Trans. Intell. Transp. Syst.*, to be published, doi: 10.1109/TITS.2020.2978438.

[32] I. Capraro *et al.*, "Impact of turbulence in long range quantum and classical communications," *Phys. Rev. Lett.*, vol. 109, Nov. 2012.

[33] A. Geiger, P. Lenz, C. Stiller, and R. Urtasun, "Vision meets robotics: The kitti dataset," *Int. J. Robot. Res.*, vol. 11, pp. 1231–1237, 2013.

[34] Z. Li *et al.*, "Super-resolution single-photon imaging at 8.2 kilometers," *Opt. Express*, vol. 28, no. 3, pp. 4076–4086, 2020.

[35] A. Pawlikowska, "Single-photon counting LiDAR for long-range three-dimensional imaging," Ph.D. theses, Dept. Phys., Inst. Photon. Quant. Sci. Heriot-Watt Univ., Edinburgh, U.K., 2016.

[36] A. Pawlikowska, A. Halimi, R. Lamb, and G. Buller, "Single-photon three-dimensional imaging at up to 10 kilometers range," *Opt. Express*, vol. 25, no. 10, pp. 11 919–11 931, 2017.

[37] M. M. Henriksson and L. Sjqvist, "Scintillation index measurement using time-correlated single-photon counting laser radar," *Opt. Eng.*, vol. 53, no. 8, pp. 081 902–1–8, 2014.

[38] M. Hulea, Z. Ghassemlooy, X. Tang, and S. Rajbhandari, "A review on effects of the atmospheric turbulence on laser beam propagation—An analytic approach," in *Proc. 10th Int. Symp. Commun. Syst., Netw. Digit. Signal Process.*, Jul. 2016, pp. 1–6.

[39] A. Ullrich and M. Pfennigbauer, "Linear LiDAR versus geiger mode lidar: impact on data properties and data quality," in *Proc. SPIE*, vol. 9832, 2014, Art. no. 983204.

[40] G. Buller and A. Wallace, "Ranging and three-dimensional imaging using time-correlated single-photon counting and point-by-point acquisition," *IEEE J. Sel. Topics Quantum Electron.*, vol. 13, no. 4, pp. 1006–1015, Jul.–Aug. 2007.

[41] J. Tachella *et al.*, "Real-time 3D reconstruction from single-photon LiDAR data using plug-and-play point cloud denoiser," *Nature Commun.*, no. 10, pp. 1–6, 2019.

[42] A. Wallace *et al.*, "Design and of evaluation of multi-spectral LiDAR for the recovery of arboreal parameters," *IEEE Trans. Geosci. Remote Sens.*, vol. 52, no. 8, pp. 4942–4954, Aug. 2014.

[43] M. Khan, S. Muhammad, M. Awan, M. Kvicera, V. Grabner, and E. Leitgeb, "Millimeter-wave and submillimeter-wave imaging for security and surveillance," *Proc. IEEE*, vol. 95, no. 8, pp. 1683–1690, Aug. 2007.

[44] Y. Yang, M. Mandehgar, and D. R. Grischkowsky, "Broadband THz signals propagate through dense fog," *IEEE Photon. Technol. Lett.*, vol. 27, no. 4, pp. 383–386, Feb. 2015.

[45] P. Sallis, C. Dannheim, C. Icking, and M. Mder, "Air pollution and fog detection through vehicular sensors," in *Proc. 8th IEEE Asia Modelling Symp.*, 2014, pp. 181–186.

[46] H. Winner, S. Hakuli, F. Lotz, and C. Singer, *Handbook of Driver Assistance Systems: Basic Information, Components and Systems for Active Safety and Comfort*. Berlin, Germany: Springer, 2016.

[47] S. S. Zang, M. Ding, D. Smith, P. Tyler, T. Rakotoarivelo, and M. Kaafar, "The impact of adverse weather conditions on autonomous vehicles," *IEEE Veh. Technol. Mag.*, vol. 14, no. 2, pp. 103–111, Jun. 2019.

[48] F. Norouzian *et al.*, "Experimental study on low-THz automotive radar signal attenuation during snowfall," *IET Radar, Sonar Navigation*, vol. 13, no. 9, pp. 1421–1427, 2019.

[49] L. Daniel, D. Phippen, E. Hoare, A. Stove, M. Cherniakov, and M. Gashinova, "Low-thz radar, LiDAR and optical imaging through artificially generated fog," in *Proc. Int. Conf. Radar Syst.*, 2017, pp. 1–4.

[50] G. Rudolph and U. Voelzke, "Three sensor types drive autonomous vehicles," *Sensors Online*, 2017.

[51] M. Kutila, P. Pyyknen, W. Ritter, O. Sawade, and B. Schufele, "Automotive LiDAR sensor development scenarios for harsh weather conditions," in *Proc. IEEE 19th Int. Conf. Intell. Transp. Syst.*, Nov. 2016, pp. 265–270.

[52] S. Hernandez-Marin, A. Wallace, and G. Gibson, "Bayesian analysis of LiDAR signals with multiple returns," *IEEE Trans. Pattern Anal. Mach. Intell.*, vol. 29, no. 12, pp. 2170–2180, Dec. 2007.

[53] A. Shamsudin, K. Ohno, T. Westfechtel, S. Takahiro, Y. Okada, and S. Tadokoro, "All weather perception: Joint data association, tracking, and classification for autonomous ground vehicles," *Adv. Robot.*, vol. 30, no. 11–12, pp. 729–743, 2016.

[54] S. Pellegrini, G. Buller, J. Smith, A. Wallace, and S. Cova, "Laser-based distance measurement using picosecond resolution time-correlated single photon counting," *Meas. Sci. Technol.*, vol. 11, no. 4, pp. 713–716, 2000.

[55] C. Mallet and F. Bretar, "Full-waveform topographic LiDAR: State-of-the art," *ISPRS J. Photogrammetry Remote Sens.*, vol. 64, no. 1, pp. 1–16, 2009.

[56] H. Wang, B. Wang, B. Liu, X. Meng, and G. Yang, "Pedestrian recognition and tracking using 3D LiDAR for autonomous vehicle," *Robot. Auton. Syst.*, vol. 88, pp. 71–78, 2017.

[57] A. Wallace, B. Liang, J. Clark, and E. Trucco, "Improving depth image acquisition using polarized light," *Int. J. Comput. Vision*, vol. 32, no. 2, pp. 87–109, 1999.

[58] A. Wallace, P. Csakany, G. Buller, and A. Walker, "3D imaging of transparent objects," in *Proc. Brit. Mach. Vision Conf.*, 2000, pp. 466–475.

[59] D. Shin, F. Xu, F. N. C. Wong, J. H. Shapiro, and V. K. Goyal, "Computational multi-depth single-photon imaging," *Opt. Express*, vol. 24, no. 3, pp. 1873–1888, Feb. 2016.

[60] M. A. Hofton, J. B. Minster, and J. B. Blair, "Decomposition of laser altimeter waveforms," *IEEE Trans. Geosci. Remote Sens.*, vol. 38, no. 4, pp. 1989–1996, Jul. 2000.

[61] A. Persson, U. Soderman, J. Topel, and S. Ahlberg, "Visualization and analysis of fullwaveform airborne laser scanner data," *Int. Arch. Photogrammetry, Remote Sens. Spatial Inf. Sci.*, vol. ISPRS WG III/3, pp. 103–108, 2005.

[62] C. Mallet, F. Lafarge, M. Roux, U. Soergel, F. Bretar, and C. Heipke, "A marked point process for modeling LiDAR waveforms," *IEEE Trans. Image Process.*, vol. 19, no. 12, pp. 3204–3221, Dec. 2010.

[63] J. Tachella *et al.*, "Bayesian 3D reconstruction of complex scenes from single-photon LiDAR data," *Siam J. Imag. Sci.*, vol. 12, pp. 521–550, 2019.

[64] S. Richardson and P. Green, "On bayesian analysis of mixtures with an unknown number of components," *J. Royal Stat. Soc. B*, vol. 59, no. 6, pp. 731–792, 2008.

[65] A. Halimi, R. Tobin, A. McCarthy, S. McLaughlin, G. Buller, and G. Stuart, "Restoration of multilayered single-photon 3D LiDAR images," in *Proc. 25th Eur. Signal Process. Conf. (EUSIPCO)*, 2017, pp. 708–712.

[66] R. Tobin *et al.*, "Long range depth profiling of camouflaged targets using single photon detection," *Opt. Eng.*, vol. 57, pp. 003 103/1–10, 2018.

[67] S. Hernandez-Marin, A. Wallace, and G. Gibson, "Multilayered 3D LiDAR image construction using spatial models in a Bayesian framework," *IEEE Trans. Pattern Anal. Mach. Intell.*, vol. 30, no. 6, pp. 1028–1040, Jun. 2008.

[68] J. Rapp and V. K. Goyal, "A few photons among many: Unmixing signal and noise for photon-efficient active imaging," *IEEE Trans. Comput. Imag.*, vol. 3, no. 3, pp. 445–459, Sep. 2017.

[69] D. B. Lindell, M. OToole, and G. Wetzstein, "Single-photon 3D imaging with deep sensor fusion," *ACM Trans. Graph. (SIGGRAPH)*, vol. 37, no. 4, pp. 1–12, 2018.

[70] W. Marais and R. Willett, "Proximal-gradient methods for poisson image reconstruction with bm3d-based regularization," in *Proc. IEEE Int. Workshop Comput. Advances Multi-Sensor Adaptive Process.*, Dec. 2017, pp. 1–5.

[71] A. Halimi, R. Tobin, A. McCarthy, J. Bioucas-Dias, S. McLaughlin, and G. S. Buller, "Robust restoration of sparse multidimensional single-photon LiDAR images," *IEEE Trans. Comput. Imag.*, vol. 6, pp. 138–152, 2020.

[72] S. Chen *et al.*, "Learning non-local spatial correlations to restore sparse 3D single-photon data," *IEEE Trans. Image Process.*, vol. 29, pp. 3119–3131, 2020.

[73] A. Halimi *et al.*, "Restoration of intensity and depth images constructed using sparse single photon data," in *Proc. 24th Eur. Signal Process. Conf. (EUSIPCO)*, 2016, pp. 86–90.

[74] P. Besl and R. Jain, "Invariant surface characteristics for 3D object recognition in range images," *Comput. Vision, Graph. Image Process.*, vol. 33, no. 1, pp. 33–80, 1986.

[75] D. Ferstl, C. Reinbacher, R. Ranftl, M. Ruther, and H. Bischof, "Image guided depth upsampling using anisotropic total generalised variation," in *Proc. Int. Conf. Comput. Vision*, 2013, pp. 993–1000.

[76] A. Maccarone *et al.*, "Underwater depth imaging using time-correlated single photon counting," *Opt. Express*, vol. 26, pp. 33 911–33 926, 2015.

[77] A. A. Maccarone, F. D. Rocca, A. McCarthy, R. Henderson, and G. Buller, "Three-dimensional imaging of stationary and moving targets in turbid underwater environments using a single-photon detector array," *Opt. Express*, vol. 27, no. 2, pp. 28 437–28 456, 2019.
[78] P. Chhabra, A. Maccarone, A. McCarthy, A. Wallace, and G. Buller, "Discriminating underwater LiDAR target signatures using sparse multispectral depth codes," in *Proc. Conf. Sensor Signal Process. Defence*, 2016, pp. 1–5.
[79] E. Charbon and S. Donati, "SPAD sensors come of age," *Opt. Photon. News*, vol. 21, no. 2, pp. 34–41, 2010.
[80] M. Albota *et al.*, "Three-dimensional imaging laser radar with a photon-counting avalanche photodiode array and microchip laser," *Appl. Opt.*, vol. 41, no. 36, pp. 7671–7678, 2002.
[81] R. Henderson *et al.*, "A 256256 40nm/90nm cmos 3D-stacked 120db dynamic-range reconfigurable time-resolved SPAD imager," in *Proc. IEEE Int. Solid- State Circuits Conf.*, 2019, pp. 106–108.
[82] X. Ren *et al.*, "High-resolution depth profiling using a range-gated si cmos spad quanta image sensor," *Opt. Express*, vol. 26, no. 5, pp. 5541–5557, 2018.
[83] S. Chan *et al.*, "Long range depth imaging using a single photon detector array and non-local data fusion," *Scientific Rep.*, vol. 9, no. 8075, pp. 1–12, 2019.
[84] G. Intermite *et al.*, "Fill factor improvement of Si CMOS single-photon avalanche diode detector arrays by integration of diffractive microlens arrays," *Opt. Express*, vol. 23, no. 26, pp. 33 777–33 791, 2015.
[85] T. Abbas, N. Dutton, O. Almer, S. Pellegrini, Y. Henrion, and R. Henderson, "Backside illuminated SPAD image sensor with 7.83m pitch in 3D-stacked CMOS technology," in *Proc. IEEE Int. Electron Devices Meeting*, 2016, pp. 8.1.1–8.1.4.
[86] L. Parmesan *et al.*, "A 256 x 256 SPAD array with in-pixel time to amplitude conversion for fluorescence lifetime imaging microscopy," in *Proc. IISW Conf.*, 2015, pp. 1–4.
[87] C. Zhang, S. Lindner, I. Antolović, J. Pavia, M. Wolf, and E. Charbon, "A 30-frames/s, 252 $\times$ 144 SPAD flash LiDAR with 1728 dual-clock 48.8-ps TDCS, and pixel-wise integrated histogramming," *IEEE J. Solid State Circuits*, vol. 54, no. 4, pp. 1137–1151, Apr. 2019.
[88] D. Bronzi, Y. Zou, F. Villa, S. Tisa, A. Tosi, and F. Zappa, "Automotive three-dimensional vision through a single-photon counting SPAD camera," *IEEE Trans. Intell. Transp. Syst.*, vol. 17, no. 3, pp. 782–794, Mar. 2016.
[89] I. Gyongy *et al.*, "1kfps time-of-flight imaging with a 3D-stacked CMOS SPAD sensor," in *Proc. Int. Image Sensor Workshop (IISW)*, 2019.
[90] M. Itzler *et al.*, "Comparison of 32 x 128 and 32 x 32 geiger-mode apd fpas for single-photon 3D ladar imaging," in *Proc. SPIE Conf.*, vol. 8033, 2011, Art. no. 80330G.
[91] M. Laurenzis, "Single photon range, intensity and photon flux imaging with kilohertz frame rate and high dynamic range," *Opt. Express*, vol. 27, no. 26, pp. 38 391–38 403, 2019.
[92] M. Henriksson and P. Jonnson, "Photon-counting panoramic three dimensional imaging using a geigermode avalanche photodiode array," *Opt. Eng.*, vol. 57, no. 9, 2018, Art. no. 093104.
[93] G. Acconcia, A. Cominelli, I. Rech, and M. Ghioni, "High-efficiency integrated readout circuit for single photon avalanche diode arrays in fluorescence lifetime imaging," *Rev. Scientific Instrum.*, vol. 87, 2016.
[94] I. Gyongy *et al.*, "High-speed particle tracking in microscopy using spad image sensors," *High-Speed Biomed. Imag. Spectrosc.*, vol. III, 2018.
[95] G. Howland, D. Lum, M. Ware, and J. Howell, "Photon counting compressive depth mapping," *Opt. Express*, vol. 21, pp. 383–399, 2013.
[96] M.-J. Sun *et al.*, "Single-pixel 3D imaging with time-based depth resolution," *Nature Commun.*, vol. 7, pp. 1–10, 2016.
[97] A. Assmann, B. Stewart, J. Mota, and A. Wallace, "Compressive super-pixel LiDAR for high frame rate 3D depth imaging," in *Proc. IEEE Global Conf. Signal Image Process.*, 2019, pp. 1–5.
[98] A. Gaidon, Q. Wang, Y. Cabon, and E. Vig, "Virtual worlds as proxy for multiobject tracking analysis," in *Proc. IEEE Conf. Comput. Vision Pattern Recognit.*, 2016, pp. 4340–4349.
[99] S. Hernandez-Marin and A. Wallace, "Profiling algorithms for detection and resolution of surface depth," in *DTC Electro-Magn. Remote Sens.*, vol. DTC-EMRS, Tech. Rep., pp. 1–21, 2007.
[100] A. Halimi, A. Maccarone, A. McCarthy, S. McLaughlin, and G. S. Buller, "Object depth profile and reflectivity restoration from sparse single-photon data acquired in underwater environments," *IEEE Trans. Comput. Imag.*, vol. 3, no. 3, pp. 472–484, Sep. 2017.
[101] A. Bhandari, A. Wallace, and R. Raskar, "Super-resolved time-of-flight sensing via fri sampling theory," in *Proc. IEEE Int. Conf. Acoust., Speech Signal Process.*, 2016, pp. 4009–4013.
[102] Y. Hua and T. Sarkar, "Matrix pencil method for estimating parameters of exponentially damped/undamped sinusoids in noise," *IEEE Trans. Acoust., Speech Signal Process.*, vol. 38, no. 5, pp. 814–824, May 1990.
[103] J. Ye, A. Wallace, A. A. Zain, and J. Thompson, "Parallel Bayesian inference of range and reflectance from LaDAR profiles," *J. Parallel Distrib. Comput.*, vol. 73, no. 4, pp. 383–399, 2013.
[104] Z.-P. Li *et al.*, "Single-photon computational 3D imaging at 45 km," 2019, *arxiv:1904.10341v1*.
[105] P. Vines *et al.*, "High performance planar germanium-on-silicon single-photon avalanche diode detectors," *Nature Commun.*, vol. 10, no. 1086, pp. 1–10, 2019.
[106] K. Kuzmenko *et al.*, "3D LiDAR imaging using Ge-on-Si single-photon avalanche diode detectors," *Opt. Express*, vol. 28, no. 2, pp. 1330–1344, 2020.
[107] R. Carrillo, A. Ramirez, G. Arce, K. Barner, and B. Sadler, "Robust compressive sensing of sparse signals: A review," *EURASIP J. Advances Signal Process.*, vol. 108, pp. 1–17, 2016.
[108] F. Zhang, P. Du, Q. Liu, M. Gong, and X. Fu, "Adaptive strategy for CPPM single-photon collision avoidance LiDAR against dynamic crosstalk," *Opt. Express*, vol. 25, no. 11, pp. 12 237–12 250, 2017.

Andrew M. Wallace received the B.Sc. and P.hD. degrees from the University of Edinburgh in 1972 and 1975 respectively. He is a Professor of signal and image processing with Heriot-Watt University. His research interests include LiDAR and 3D vision, image and signal processing, and accelrated computing. He has published extensively, receiving a number of best paper and other awards, and has secured funding from EPSRC, the EU and other industrial and government sponsors. He is a Chartered Engineer and a fellow of the Institute of Engineering Technology.

Abderrahim Halimi received the E.ng. degree in electronics from the National Polytechnic School of Algiers, Algeria, in 2009, and the M.Sc. and Ph.D. degrees in signal processing from the Institut National Polytechnique de Toulouse, France, in 2010 and 2013, respectively. He was a Post-doctoral Research Associate from 2013 to 2018, and is currently an Assistant Professor and Royal Academy of Engineering (RAEng) Research Fellow within the School of Engineering and Physical Sciences at Heriot-Watt University. His research activities focus on statistical signal and image processing, with a particular interest in Bayesian inverse problems, applied to remote sensing (hyperspectral imaging, satellite altimetry), single-photon depth and medical imaging.

Gerald S. Buller received the B.Sc. degree in natural philosophy from the University of Glasgow in 1986, and the Ph.D. degree in physics from Heriot-Watt University in Edinburgh, U.K., in 1989, where he is currently a Professor of physics. In 2002, he founded Helia Photonics, Ltd., where he remains company Chairman. His research interests include aspects of single-photon detection, including short-wave infrared single-photon detectors, quantum communications and quantum enhanced imaging. In 2015, Prof. Buller was awarded an EPSRC Established Career Fellowship in Quantum Technology. He is a fellow of the Institute of Physics, a fellow of the Optical Society of America and a fellow of the Royal Society of Edinburgh.